Met. Mater. Int., Vol. 23, No. 1 (2017), pp. 115~125
doi: 10.1007/s12540-017-6356-y

Effect of W on Stress Corrosion Cracking Susceptibility of Newly Developed Ni-Saving Duplex Stainless Steels

Heon-Young Ha[1,*], Tae-Ho Lee[1], and Sangshik Kim[2,*]

[1]Metallic Materials Devision, Korea Institute of Materials Science, Changwon 51508, Republic of Korea
[2]Department of Materials Engineering and Convergence Technology, Research Center for Aircraft Part Technology, Gyeongsang National University, Chinju 52828, Republic of Korea

(received date: 20 May 2016 / accepted date: 22 August 2016)

Effect of W on stress corrosion cracking behavior (SCC) of Ni-saving duplex stainless steels (Fe18Cr6Mn3Mo0.4N (2.13, 5.27)W, in wt%) was investigated in 4 M NaCl solution using a slow strain rate test method. The change in the W content from 2.13 to 5.27 wt% marginally affected the tensile properties of the investigated DSSs. Alloying W clearly improved the pitting initiation resistance and repassivation tendency of the investigated alloys, but the SCC susceptibility was not remarkably decreased by addition of W. The slight enhancement in the SCC resistance of the alloy containing 5.27 wt% W was revealed to be correlated with the accelerated galvanic corrosion between the ferrite and austenite phases as a result of the W partitioning preferentially into the ferrite phase which could encourage the propagation of pitting.

Keywords: alloys, corrosion, tensile test, stress corrosion cracking, galvanic corrosion

1. INTRODUCTION

Duplex stainless steels (DSSs) consisted of balanced proportions of the austenite (γ) and ferrite (α) phases are attractive structural materials due to its good mechanical properties and desirable corrosion resistance including stress corrosion cracking (SCC) resistance [1-10]. The DSSs are therefore widely used where both corrosion resistance and high strength are required, such as chemical tankers, desalination plants, chemical and petrochemical processes, pipelines and oil and gas separators [1,3,4,6,7,9]. Recent development strategies of DSSs can be roughly classified into two categories [3,5,6,8,11,12]: one is super DSS grade exhibiting excellent corrosion resistance (pitting resistance equivalent number (PREN) ≥ 40, where PREN = [Cr]+3.3[Mo]-[Mn]+16[N], in wt%) [13-15]), and the other is lean DSS grade having the moderate corrosion resistance comparable to that of AISI 304 stainless steels [11,16-20]. For the lean DSSs, Mn and N are actively used in replacement of Ni to stabilize the g phase, thus the price stability of the alloys can be achieved [11,16-20]. Recently, the present authors developed new cost-effective DSSs [21], which comprising 16.5-19.5 wt% Cr, 2.5-3.5 wt% Mo, 1.0-5.5 wt% W, 5.5-7.0 wt% Mn, 0.35-0.45 wt% N, with balanced Fe.

W is a α-stabilizing element and known to be beneficial to mechanical properties by the solid solution hardening and grain refinement in Fe-based alloys [22,23]. In addition, it is reported that the W retards the recovery of the dislocation and recrystallization rate upon tempering because W inhibits the diffusion of Fe atoms [24]. Particularly in the newly developed DSSs, W was generally added to improve localized corrosion resistance including pitting corrosion and the SCC [23,25-29]. W is often used into DSSs in order to partially substitute for Mo, because W tends to retard precipitations including sigma phase resulting in improving the resistance to localized corrosion [18,30-34]. Moreover, it is reported that the enhanced resistance to pitting corrosion by the alloying W is attributed to the formation of stable passive film assisted by forming WO_3 in the passive film [25,27,28]. In addition, the alloyed W is also reported to form WO_4^{2-} ion inside the passive film which can decrease the ion migration in the passive layer [27].

Meanwhile, the effect of W addition on SCC of DSSs is still arguable. Therefore, in this study, the SCC behavior of the newly developed DSSs with different W contents of 2.13 and 5.27 wt% was investigated in an aqueous NaCl environment under applied potentials using a slow strain rate test (SSRT) method. The effect of W on the SCC susceptibility was assessed based on the micrographic as well as the fractographic observation, and the results were discussed in terms of the electrochemical behavior of the alloys.

2. EXPERIMENTAL PROCEDURE

The designation and chemical compositions of the investigated

*Corresponding author: hyha2007@kims.re.kr, sang@gnu.ac.kr

Table 1. Chemical compositions (in wt%) and PREN values of the investigated duplex stainless steels

Alloy	Fe	Cr	Ni	Mn	Mo	N	W	C	P	Si	S	PREN*
D2W	Balance	18.80	0.60	6.75	2.92	0.44	2.13	0.014	0.004	0.14	0.004	32.56
D5W	Balance	17.24	0.50	6.03	2.50	0.41	5.27	0.013	0.003	0.13	0.004	34.72

*PREN=[Cr]+3.3×[Mo]+1.65×[W]+16×[N]-[Mn], in wt%

alloys are given in Table 1. The ingots (10 kg) of the alloys were fabricated using a pressurized induction melting furnace (VIM 4 III-P, ALD). The ingots were homogenized and then hot rolled into plates with a thickness of 4 mm followed by water quenching. The hot-rolled plates of the D2W and D5W alloys were solutionized at 1220 and 1130 ℃ for 30 min, respectively, in order to make the duplex microstructure with equal volume fractions of α and γ phases. The solutionization temperatures were determined based on thermodynamic calculation (Thermo-Calc. version 4.0, TCFE 7 database). Microstructures of the alloys were examined using an optical microscope and a scanning electron microscope (SEM, JSM-5800, JEOL). In addition, the chemical compositions of the α and γ phases in the annealed samples were investigated using an electron probe micro analysis with a wavelength dispersive spectrometry (EPMA-WDS, JXA-8530F, JEOL). For the micrographic observations, the specimens were polished up to 1 μm using diamond suspension and etched in a solution of 15 mL HCl and 85 mL ethanol for 45 min. The phase fractions of the annealed samples were quantitatively analyzed on the optical micrographs using an image analyzer. Then, the normal deformation behavior of the specimens was investigated using tensile tests conducted at a nominal strain rate of 10^{-3} s^{-1} in air at 25 ℃.

SCC susceptibility of the alloys was evaluated using an SSRT method on a constant extension rate test machine (R&B model, T07-025) combined with a 3-electrode electrochemical cell in accordance with ASTM G129 [35]. The electrochemical cell consisted of a specimen as a working electrode, a Pt counter electrode, and an Ag/AgCl reference electrode. For the SSRT, the tensile specimens with a gauge length of 24 mm and a diameter of 3.8 mm were prepared from 4 mm thick plate parallel to rolling direction. Each specimen was ground using SiC paper up to a 1200-grit. The SSRTs were conducted in a 4 M NaCl solution at 80 ℃ at an anodic applied potential of +0.05 V versus corrosion potential (E_{corr}) at a nominal strain rate of 10^{-6} s^{-1} [36-38]. As reference data, the SSRTs were also performed on each specimen in air at 25 ℃ (relative humidity: 45-55%) under the same strain rate of 10^{-6} s^{-1}. SCC susceptibility was then quantified based on the SSRT results obtained in air and aqueous chloride environments. After the SSRT, the fracture surface of the tested specimen was observed by the SEM to understand the fracture mode and the SCC mechanisms.

The SCC susceptibility of the alloys was interpreted in correlation with the electrochemical behavior of the alloys. The pitting corrosion resistance of the alloys was evaluated by measuring the pitting potential (E_{pit}) and repassivation potential (E_{rp}) using a cyclic potentiodynamic polarization test in the 4 M NaCl solution at 80 ℃. In addition, the general corrosion behavior and critical dissolution current density (i_{crit}) of the alloys were examined using a linear polarization tests in 4 M NaCl+0.02 M HCl solution at 80 ℃ (pH 1.41). For the polarization tests, the specimens were ground using SiC paper up to 2000-grit, and the exposed area was controlled to be 0.13 cm^2 using electroplating tape. After the polarization tests, it was confirmed that the no crevice corrosion occurred. Finally, the pit initiation sites and galvanic corrosion behavior of the alloys was investigated. The specimens which were polished to 1 μm using diamond suspension were immersed in a 4 M NaCl+0.1 M HCl (pH 1.17) solution at 80 ℃ for 20 min. After the immersion, the corroded topography was investigated using the SEM and a surface optical profiler (Wyko NT8000, Veeco [39,40]). The SSRT was conducted at least in duplicate, and the polarization tests and the immersion tests were carried out at least 3 times, and good reproducibility was confirmed.

3. RESULTS AND DISCUSSION

3.1. Microstructural analysis

Figure 1 shows three-dimensional optical micrographs (Figs. 1(a) and 1(b)) of the D2W and D5W alloys, respectively. The elongated bands of the γ (shown as a relatively dark phase in Figs. 1(a) and 1(b)) and the α phases were observed in both alloys. The image analyses on the optical micrographs indicated that the volume fractions of the α phase of the D2W and D5W alloys were 47.0 and 48.2 vol%, respectively. The micrographs show that precipitations including carbide and/or nitride and intermetallic phases are not formed in the two alloys. Average grain sizes of the two alloys are similar to each other having 30-35 μm in a diameter.

3.2. Stress-strain behavior

Figure 2(a) shows the representative stress-strain curves of the D2W and D5W alloys measured in air at a strain rate of 10^{-3} s^{-1}. The change in the W content from 2.13 to 5.27 wt% marginally affected the tensile properties of the investigated DSSs. Slight increases in yield and tensile strengths along with a marginal decrease in tensile elongation were observed with increasing the W content (Table 2 and Fig. 2(a)). Figures 2(b)-2(e) are the SEM fractographs of the tensile-tested D2W and D5W alloys. As marked by the dotted rectangles in the low-magnification fractographs (Figs. 2(b) and 2(d)), Figs. 2(c) and 2(e) were both taken in the fibrous zone (center area of

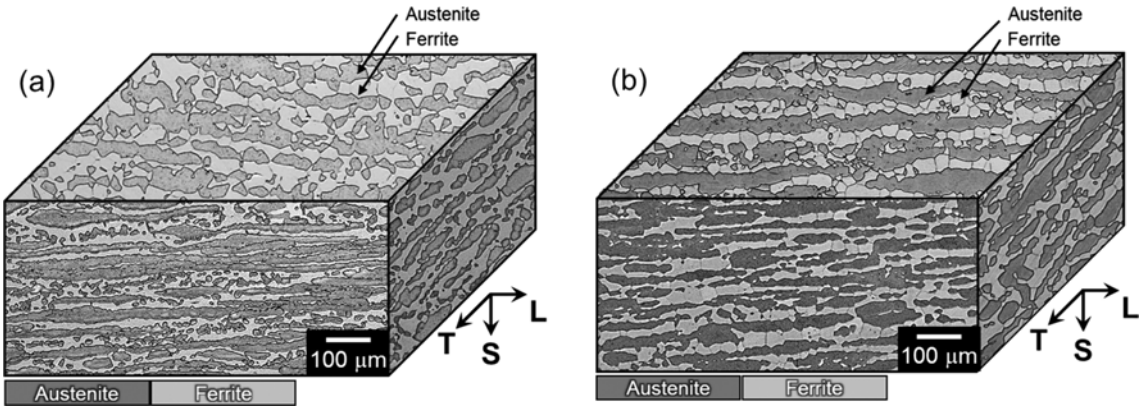

Fig. 1. Three-dimensional optical micrographs of the (a) D2W and (c) D5W alloys.

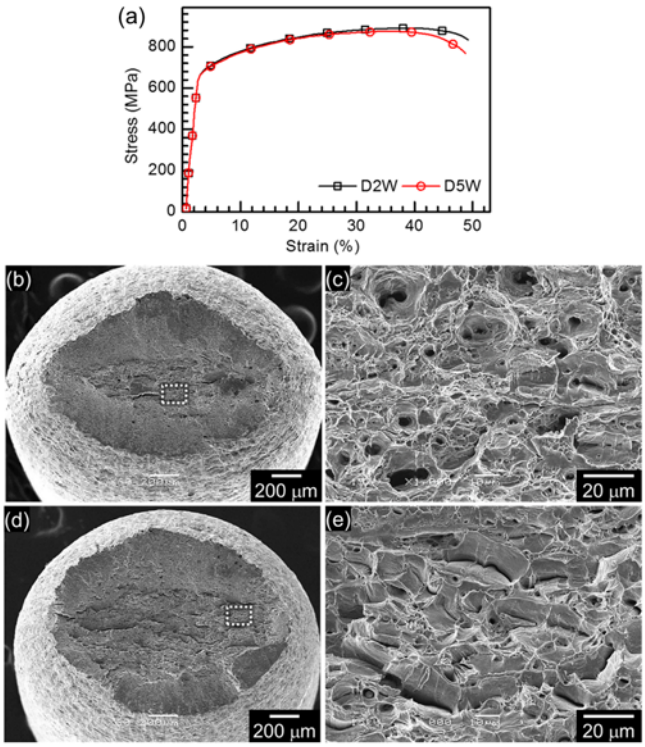

Fig. 2. (a) Stress-strain curves of D2W and D5W alloys in air at 25 °C at a strain rate of 10^{-3} s^{-1}. SEM fractographs of the (b), (c) D2W alloy (low and high magnification, respectively) and the (d), (e) D5W alloy (low and high magnification, respectively).

Table 2. Tensile properties of the D2W and D5W alloys measured in air at 25 °C at a strain rate of 10^{-3} s^{-1}

Alloy	Yield strength, (MPa)	Tensile strength, (MPa)	Tensile elongation, (%)
D2W	631	880	45.5
D5W	648	902	45.0

the round tensile specimen). In both alloys, the dimple rupture mode prevailed. For the D2W alloy (Figs. 2(b) and 2(c)), bimodal distribution of dimples was observed. The isolated γ colonies could probably provide the initiation sites for the relatively large dimples. The increase in W content tended to encourage the cleavage mode of tensile fracture in the DSSs, as shown in Figs. 2(d) and 2(e).

3.3. Pitting corrosion resistance

Figure 3 shows the cyclic polarization curves of D2W and D5W alloys, which were measured in the 4 M NaCl solution at 80 °C at a potential sweep rate of 2 mV s^{-1}. The E_{corr} values of the D2W and D5W alloys were -0.39 and -0.40 $V_{Ag/AgCl}$, respectively, and it was shown that the passive potential range was extended from the E_{corr} to the E_{pit} (Fig. 3(a)). The average E_{pit} and E_{rp} values of the alloys obtained from 5 repeated tests are presented in Fig. 3(b). The E_{rp} was determined as a cross-over potential in the cyclic polarization curve exhibiting the hysteresis loop as shown in Fig. 3(a) [41]. The average E_{pit} value of the D2W alloy was -0.192±0.0056 $V_{Ag/AgCl}$ and that of the D5W alloy was -0.0632±0.0334 $V_{Ag/AgCl}$. In addition, the average E_{rp} values of the D2W and D5W alloys were -0.339±0.0196 and -0.258±0.0234 $V_{Ag/AgCl}$, respectively. In Fig. 3(b), the slope of the E_{pit} versus W content ([W]) graph (dE_{pit}/d[W]) was 0.0373 V wt%$^{-1}$, and that of the E_{rp} versus the [W] graph (dE_{rp}/d[W]) was 0.0225 V wt%$^{-1}$. The dE_{rp}/d[W] value was slightly smaller than the dE_{pit}/d[W] value.

Figure 3 demonstrates that the D5W alloy has higher resistance to pit initiation than the D2W alloy, and it also manifests that the broken passive film of the D5W alloy is possible to be repaired at the higher potential (i.e., under the more oxidizing condition) than the D2W alloy. In the D2W alloy, the concentrations of Cr, Mo, and N, which are known to be beneficial to the resistance to pitting corrosion, were slightly higher than those of the D5W alloy as shown in Table 1. Thus, it is considered that the alloying W plays a decisive role in a rise in the E_{pit} and E_{rp} values of the two investigated alloys, even in the precipitate-free matrices.

Another notable point requires attention in Fig. 3(a): the amount of consumed charge during the period between pit initiation and repassivation, which can be compared by the size of the loop in the cyclic polarization curves. The D2W alloy

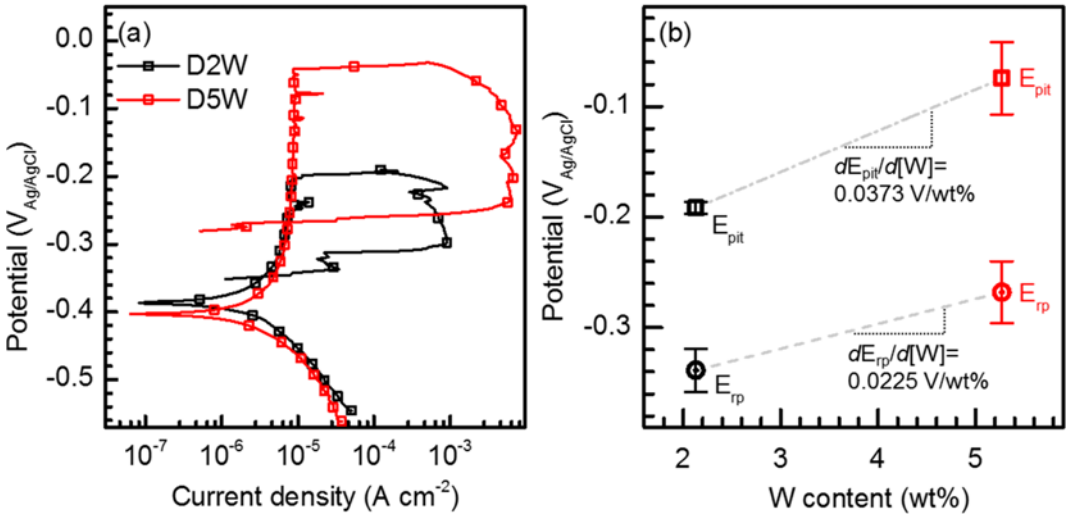

Fig. 3. (a) Cyclic polarization curves of the D2W and D5W alloys measured in 4 M NaCl solution at 80 °C at a potential sweep rate of 2 mV s^{-1}. (b) Variations in the average E_{pit} and E_{rp} values of the alloys as a function of the W content.

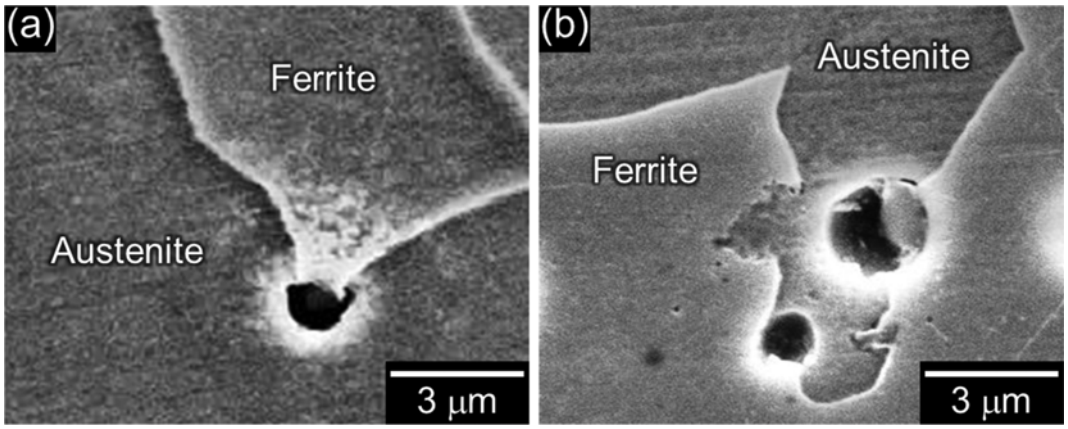

Fig. 4. SEM micrographs of pit initiation sites of the (a) D2W and (b) D5W alloys after immersion in 4 M NaCl+0.01 M HCl solution.

shows the maximum dissolution current density of approximately 0.8-1.0 mA cm^{-2} (at -0.3 $V_{Ag/AgCl}$), but that of the D5W alloy is much larger showing approximately 5.2-7.2 mA cm^{-2} (at -0.2 $V_{Ag/AgCl}$). This feature is correlated well with the smaller value of dE_{rp}/d[W] than the dE_{pit}/d[W].

Then, the pit initiation sites were investigated using a SEM after an immersion test in 4 M NaCl+0.1 M HCl solution. The acidified chloride solution was used for this test in order to simultaneously identify the pit initiation sites and the phase boundary. In both alloys, the pitting mostly initiated in the γ phase adjacent to the a phase and propagated into the γ phase as shown in Fig. 4.

3.4. SCC susceptibility

SCC susceptibility was assessed using the SSRT in air at 25 °C and in the 4 M NaCl solution at 80 °C under an anodic applied potential. The applied potential values for the latter experiment was determined to be +0.05 V versus the E_{corr} the alloys based on the polarization curves shown in Fig. 3(a). The anodic applied potential for the SSRT was required to exclude the influences of H and/or H_2 on the SCC during the SSRT. In addition, it was possible to accelerate the SCC by applying the anodic potential. However, the applied potential should be lower than the E_{rp} in order to minimize the influence of pure pitting corrosion on SCC. For this reasons, the applied potential was determined as +0.05 V versus E_{corr} [42-44]. The E_{corr} of the D2W and D5W alloys were -0.39 and -0.40 $V_{Ag/AgCl}$, respectively, thus the applied potentials for the D2W and D5W alloys were -0.34 and -0.35 $V_{Ag/AgCl}$, respectively (Table 3).

Figures 5(a) and 5(b) show the representative stress-strain curves of D2W and D5W alloys, respectively, measured in air at 25 °C and 4 M NaCl solution at 80 °C (strain rate=10^{-6} s^{-1}). Table 3 summarizes the SSRT results, and the average values were obtained from at least duplicate test results. In this table, the SCC susceptibility was expressed by the reduction ratio of tensile elongation (RTE) in SCC-causing environment with respect to that in inert environment (*i.e.*, air in this study) [37,38,45]. As shown in Fig. 5, the D2W and D5W

Table 3. Slow strain rate test results of the D2W and D5W alloys at a strain rate of 10^{-6} s^{-1} in air at 25 °C and 4 M NaCl solution at 80 °C under anodic applied potential (+0.05 V versus E_{corr})

Alloy	Test condition	Applied potential ($V_{Ag/AgCl}$)	Yield strength (MPa)	Tensile strength (MPa)	Tensile elongation (%)	Tensile elongation RTE* (%)	Time to failure (h)
D2W	Air, 25 °C	-	556	811	35.8	-	110
	4 M NaCl, 80 °C	-0.34	506	780	23.1	35.5	74
D5W	Air, 25 °C	-	597	850	37.1	-	115
	4 M NaCl, 80 °C	-0.35	524	808	25.0	32.6	82

*RTE: Reduction ratio of tensile elongation

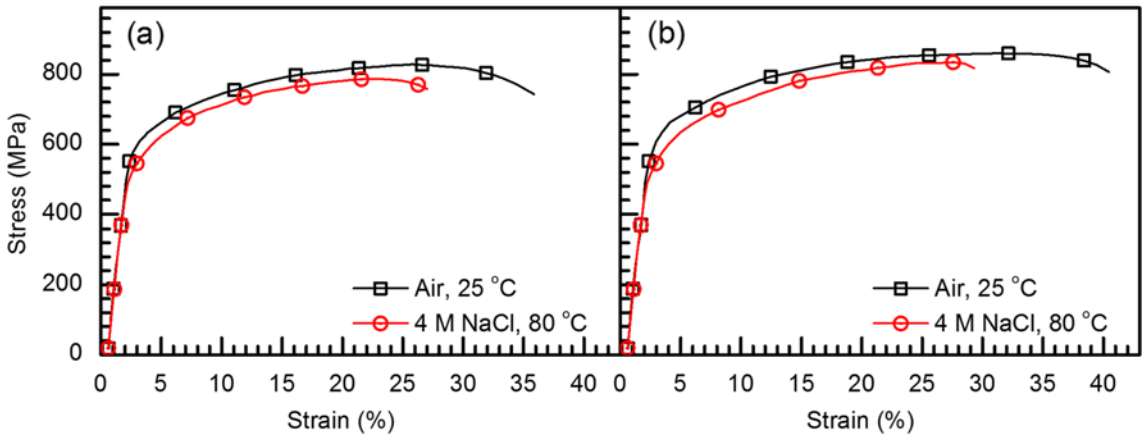

Fig. 5. Stress-strain curves of the (a) D2W and (b) D5W alloys measured in air at 25 °C and 4 M NaCl solution at 80 °C under an anodic applied potential. The strain rate was 10^{-6} s^{-1}.

alloys were susceptible to SCC in the 4 M NaCl solution at 80 °C under the anodic applied potential, showing the RTE of 35.5 and 32.6%, respectively. It was noted that the D5W alloy containing higher W content showed marginally better resistance to SCC under this condition.

Previously, the present authors found that the fracture morphology including the site of crack initiation (*i.e.*, surface or internal) and the fracture mode (*i.e.*, cleavage or intergranular cracking) of the SSRTed specimen were important to understand the SCC behavior [37,38,45,46]. Figures 6(a) and 6(b) exhibit low and high magnification SEM fractographs of the D2W and D5W alloys, respectively, tested in air at 25 °C a strain rate of 10^{-6} s^{-1}. Unlike those shown in Fig. 2 at a higher strain rate of 10^{-3} s^{-1}, the tensile fracture for both alloys began at the surface rather than in the middle of the specimens at a strain rate of 10^{-6} s^{-1} (refer to the insets of Fig. 6). It was therefore suggested that, at a strain rate of 10^{-6} s^{-1}, both alloys were not immune to SCC in the air environment. In the area where the crack began, the cleavage facets in the α phase, along with ductile tearing between these facets,

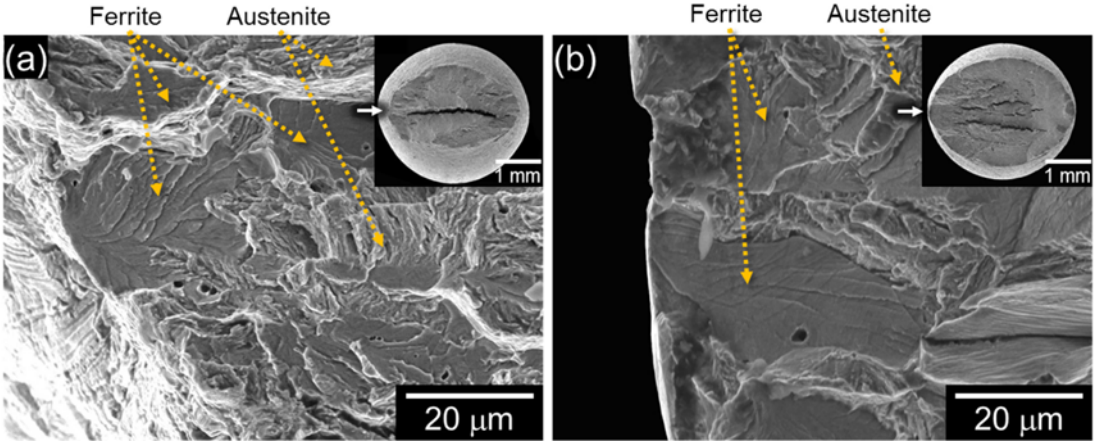

Fig. 6. SEM fractographs of the (a) D2W and (b) D5W alloys slow strain rate tested in air at 25 °C at a strain rate of 10^{-6} s^{-1}.

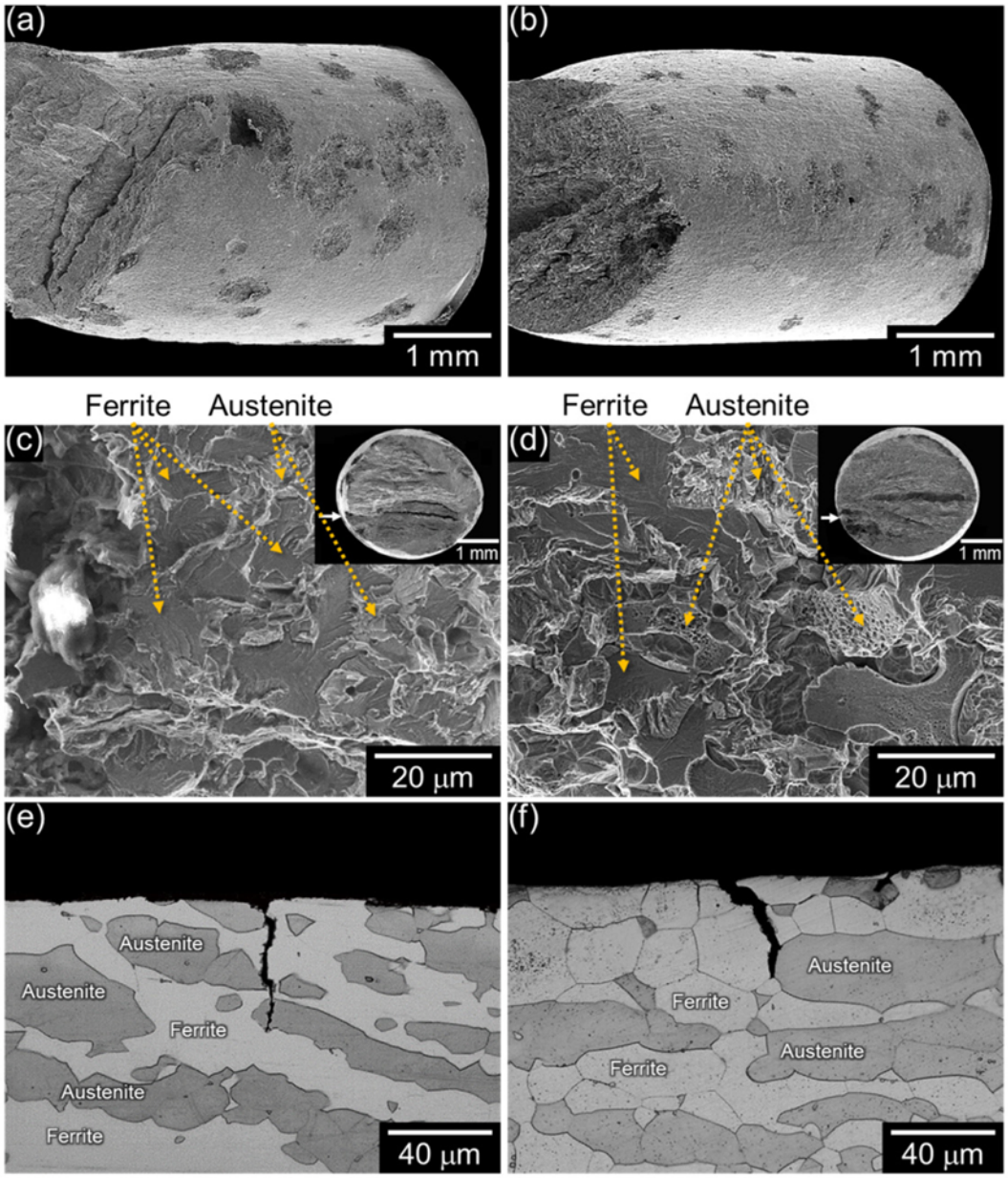

Fig. 7. SEM micrographs of the side surfaces of the (a) D2W and (b) D5W alloys, and SEM fractographs of the (c) D2W and (b) D5W alloys slow strain rate tested in 4 M NaCl solution at 80 °C at a strain rate of 10^{-6} s^{-1} under an anodic applied potential. Cross sectional views of the tested samples, (e) D2W and (f) D5W alloys.

were observed. It is notable that the boundary between these facets was much clearer for the D5W alloy than the D2W alloy.

Figures 7(a) and 7(b) are the SEM images of side surfaces of the D2W and D5W alloys, respectively, tested in the 4 M NaCl solution at 80 °C at a strain rate of 10^{-6} s^{-1} under an anodic applied potential of +0.05 V versus the E_{corr}. They clearly showed that the formation of pits was significantly suppressed with increasing the W content, which is successfully explained by the results from the polarization tests measured in the same solution (Fig. 3). It is shown that one of the pits on the specimen's surface provided the initiation site for SCC. Figures 7(c) and 7(d) are SEM fractographs of the D2W and D5W alloys, respectively, and the crack initiation sites are marked in the insets of Figs. 7(c) and 7(d). For the D2W alloy (Fig. 7(c)), relatively large cleavage facets in the α phase were observed. The γ phase between these cleavage facets in the α phase also showed the cleavage-like fracture mode. The cleavage faceting in the α phase, while the ductile tearing in the γ phase, was observed for the D5W alloy (Fig. 7(d)). The secondary cracks were often observed along the phase boundary between the α and γ. Figures 7(e) and 7(f) show the cross-sectional view of the tested D2W and D5W specimens,

respectively, in which the relatively dark phase is the γ phase. These figures suggest that the SCC in aqueous chloride solution under an anodic applied potential is frequently initiated at the phase boundaries between the α and γ for the DSSs. In the D2W alloy (Fig. 7(e)), the cracks tended to either by-pass the γ phase or cut through the γ phase. As a result of this, quasi-cleavage fracture in the γ phase was observed in between large cleavage facets in the α phase for the D2W alloy as shown in Fig. 7(c). For the D5W alloy (Fig. 7(f)), two points required attention. First, the propagation of the stress corrosion cracks through the α phase showed a tendency to follow the α grain boundary. The intergranular nature of crack propagation in the α phase and secondary cracks along the phase boundaries were therefore observed on the fracture surface of D5W alloy (Fig. 7(d)). Second, the propagation of crack tended to be blocked by the presence of γ phase. Resultantly, the tearing mode of fracture was observed, probably along the phase boundaries between α and γ, in between the large and well-developed cleavage facets in the D5W alloy.

The results from Figs. 5 to 7 can be summarized as follows: both D2W and D5W alloys were susceptible to SCC in the 4 M NaCl at 80 °C under the anodic applied potential, and the increase in the W content was marginally beneficial in improving the resistance to SCC. The electrochemical studies (Fig. 3) indicated that the increase in the W content was clearly beneficial in increasing both E_{pit} and E_{rp} of the investigated DSSs. Fractographs (Fig. 7) showed that the SCC was initiated at the pits formed on the surface. Therefore, the improved resistance to pitting corrosion initiation and the repassivation tendency with the addition of W was expected to reduce the SCC susceptibility intrinsically [37,38]. However, the improvement in the SCC resistance with the increase in W content was not so large.

3.5. Pitting resistance equivalent number

In order to understand the marginal improvement of the resistance to SCC by W addition despite the higher resistance to pitting corrosion of the D5W alloy than the D2W, the PREN values of the two constituent phases, α and γ, were investigated.

The resistance to pitting corrosion of stainless steel can be generally evaluated through PREN. The PREN is an empirical measure to estimate the pitting corrosion resistance level of stainless steels. The PREN is a function of alloying elements affecting pitting corrosion resistance, those are Cr, Mo, W, Mn, and N. Among the elements, Cr, Mo, and W are stabilizers for the α phase, and Mn and N are those for the γ phase. In DSS, the α and the γ phases are enriched with their stabilizers, respectively, and thus the PREN values of the two constituent phases become different. Previous researchers [47-51] explained that the overall resistance to the pitting corrosion of the various DSSs was determined by the pitting susceptibility level of less resistant phase than the other, which was predicted by the PREN values. In addition, the experimental evidences supported that the higher pitting corrosion resistance was achieved in the DSS which exhibits the lower difference in the PREN values between the α and γ phases, that is, $\Delta|PREN_{\alpha}-PREN_{\gamma}|$.

Therefore, the PREN values of the α and the γ phases of the D2W and D5W alloys were calculated. For stainless steels, the generally accepted PREN formula is as follows:

$$PREN = [Cr]+3.3[Mo]+1.65[W]+16[N]-[Mn]$$ [40,52,53]

For the α and γ phases of the D2W and D5W alloys, chemical compositions of the 30 points were analyzed using the EPMA, and the average compositions of the alloying elements, Ni, Mn, N, Cr, Mo, and W are presented in Table 4. Based on the results, the PREN values of the two constituent phases of the D2W and D5W alloys were calculated.

Table 4 clearly demonstrates the alloying element partitioning in the investigated DSSs. That is, the γ-stabilizers, Ni, Mn, and N, are enriched in the γ phase, and the α-stabilizers, Mo and W, are enriched in the α phase in both alloys. Most of N is concentrated in the γ phase for the D2W and D5W alloys, because of the low solubility of N in the α phase less than 0.05 wt% [40,49,53-55]. A notable point is that the concentration of Cr is slightly higher in the γ phase in both D2W and D5W alloys even though the Cr is α-stabilizer. It is considered that the reason for this phenomenon is due to the strong affinity between the N and Cr.

The PREN values of the α and γ phases of the D2W alloy are 28.01±0.999 and 32.20±1.435, respectively, and those of the D5W alloy are 31.61±0.895 and 36.42±1.981, respectively. Higher PREN values were obtained in the D5W alloy than the D2W alloy. The higher PREN value of the D5W alloy is primarily attributed to the intrinsic effect of W, and the polar-

Table 4. Chemical compositions and PREN values of the ferrite (α) and austenite (γ) phases of the D2W and D5W alloys measured using an electron probe micro analysis with a wavelength dispersive spectrometry

Alloy	phase	Composition, average ± standard deviation, wt%						PREN*
		Ni	Mn	N	Cr	Mo	W	
D2W	α	0.470±0.019	6.534±0.091	0.034±0.057	19.244±0.165	3.175±0.052	2.589±0.059	28.005±0.999
	γ	0.741±0.030	7.540±0.096	0.557±0.084	19.491±0.263	2.560±0.056	1.755±0.078	32.199±1.435
D5W	α	0.486±0.025	5.972±0.145	0.036±0.047	16.992±0.199	2.785±0.091	6.562±0.100	31.606±0.895
	γ	0.751±0.032	6.822±0.085	0.608±0.118	17.668±0.239	2.374±0.041	4.858±0.085	36.418±1.981

*PREN=Cr+3.3Mo+1.65W+16N-Mn

ization curves (Fig. 3) also support the improved resistance to pitting corrosion by W addition. It is noted that the PREN of the γ phase is higher than that of the α phase in both alloys, which is primarily due to the N enrichment. However, as shown in Fig. 4, most stable pits were observed in the γ side though the γ phase exhibited the higher PREN value. This observation indicates that the PREN values of the constituent phases, α and γ, alone cannot explain the observed SCC behavior of the investigated DSSs.

3.6. General corrosion resistance

The reason for the discrepancy between the measured and expected SCC susceptibility of the two alloys can be found in general (or uniform) corrosion rate and galvanic corrosion resistance between the α and γ phases. The notable point in Fig. 3 is the large-sized loop shown in the cyclic polarization curve of the D5W alloy in comparison with that of the D2W alloy, which implies that the dissolution rate of the matrix by general corrosion after the passive film breakdown is higher in the D5W alloy than in the D2W alloy. The E_{pit} and E_{rp} are related to pit (or crack) initiation and recovery probabilities, respectively, while the general corrosion rate has strong correlation with the pit (or crack) growth rate.

Thus, the active dissolution rates of the two alloys are compared. Figure 8(a) shows polarization curves of the D2W and D5W alloys measured in 4 M NaCl+0.02 M HCl solution at 80 °C (pH 1.41). In this test, the acidified NaCl solution was chosen for two reasons: in order to simulate the acidified environment inside the pit [41,56], and to induce the general corrosion of the bare metal surface. During the polarization test in this acidified NaCl solution, the general corrosion (or active dissolution) occurred in both alloys above their E_{corr} values showing the i_{crit} of bigger than approximately 2 mA cm^{-2} (at -0.57 $V_{Ag/AgCl}$) [57]. Comparing the E_{pit}, it is confirmed again that the D2W alloy has lower pitting corrosion resistance than the D5W alloy.

From the E_{corr} to -0.57 $V_{Ag/AgCl}$ (*i.e.*, primary passive potential, E_{PP}), the two alloys underwent active dissolution, and, above the E_{PP}, they were passivated. The average i_{crit} value at -0.57 $V_{Ag/AgCl}$ of the D5W alloy (3.195 mA cm^{-2}) is higher than that of the D2W alloy (2.075 mA cm^{-2}) as shown in Fig. 8(b). Based on this result, it is conceivable that the larger-sized loop shown in the cyclic polarization curves of the D5W alloy (Fig. 3(a)) than that of the D2W alloy is due to the higher active dissolution rate of bare metal surface inside the pit.

3.7. Galvanic corrosion resistance

General corrosion of DSS is accompanied by galvanic corrosion between the two constituent phases, α and γ. Thus, the galvanic corrosion resistance of the D2W and D5W alloys was also investigated. For this, the two alloy samples were immersed in a 4 M NaCl+0.1 M HCl (pH 1.17) solution at 80 °C for 20 min and then corrosion topography were examined using a surface optical profiler [39,40]. In order to induce general corrosion under open circuit condition (*i.e.*, without external applied potential), the immersion test was carried out in the stronger acidic solution than that used in the linear polarization tests (Fig. 8).

The corrosion topographs of the D2W and D5W alloys are presented in Fig. 9(a) and 9(b), respectively. In both alloys, corrosion rates of the two constituent phases were different, and more dissolved phase was revealed to be the γ. This observation that the γ is the less noble phase than the α in this lean DSSs is different results from the commercial DSS, such as UNS S32205 [40] and UNS S32750 [58] DSSs. For example, in the UNS S32205 and UNS S32750 alloys containing approximately 5 and 7 wt% Ni, respectively, the nobler phase is the γ phase due to the enrichment of Ni into the γ phase. In con-

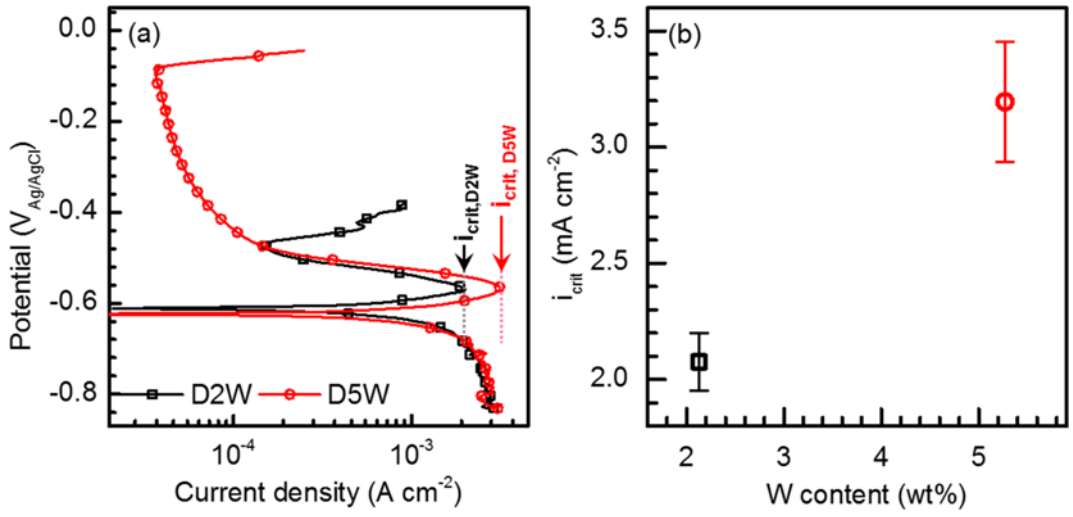

Fig. 8. (a) Linear polarization curves of the D2W and D5W alloys measured in 4 M NaCl+0.02 M HCl solution at 80 °C (pH 1.41) at a potential sweep rate of 2 mV s^{-1}. (b) Variation in the average i_{crit} values of the alloys as a function of the W content.

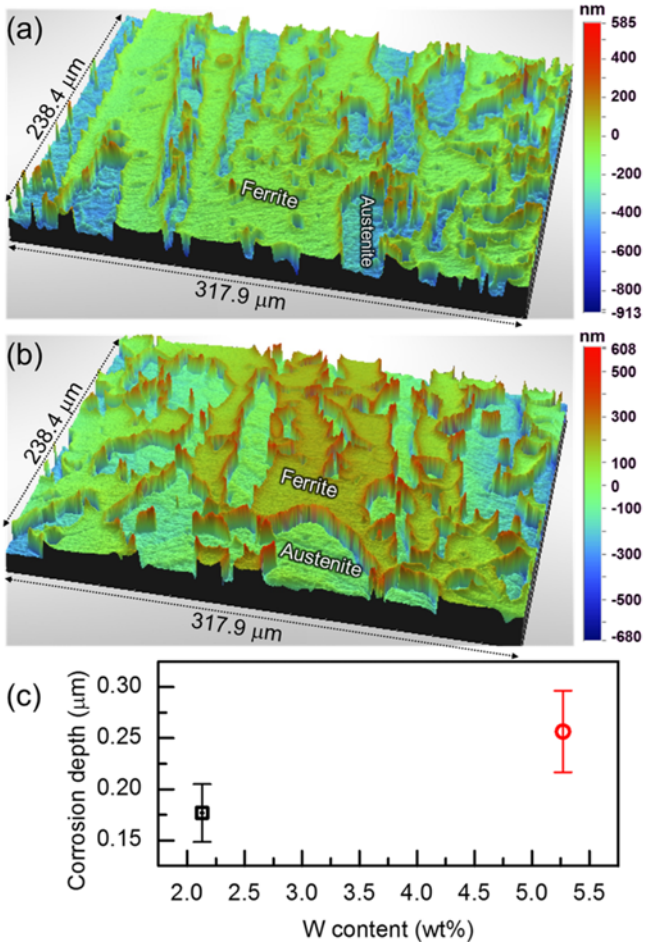

Fig. 9. 3-dimensional topographs of galvanically corroded surfaces of the (a) D2W and (b) D5W alloys. (c) Variation in the average corrosion depths of the alloys as a function of the W content.

trast, the investigated lean DSSs contain less than 1 wt% Ni, thus the γ phase is less noble than the α phase. In addition, the Ni and Mo contents of the D2W alloy is similar to those of the D5W alloy, thus the degree of nobility of the constituent phases is primarily determined by W. The corrosion depth of the γ phase relative to the α phase's surface level can reflect the relative corrosion rate of the γ phase, thus the galvanic corrosion rate can be compared by using the corrosion depth measurement [40,53]. Figure 9(c) presents the corrosion depths difference between the α and γ phases of the two alloys, and that of the D2W alloy is 0.177±0.028 μm and that of D5W alloy is 0.257±0.039 μm. The higher corrosion depth of the D5W alloy demonstrates that the galvanic corrosion resistance is lower in the D5W alloy than the D2W. It is considered that the lower galvanic corrosion resistance of the D5W alloy is attributed to the larger amount of W than the D2W alloy. Because the alloying element W is a strong α stabilizer, relatively greater amount of W is expected to be partitioned into the α phase in the investigated DSSs. Indeed, the W content of the α and γ phases in the D2W alloy are 1.755 and 2.589 wt%, respectively, and those of the α and γ phases in the D5W alloy are 4.585 and 6.565 wt%, respectively (Table 4). Thus, the difference in the W content between the α and γ phases is 0.834 for the D2W alloy and 1.704 for the D5W alloy. The D5W alloy exhibits larger difference in the W content than the D2W alloy.

The lower galvanic corrosion resistance of the D5W alloy can explain its higher i_{crit} value shown in the polarization curves in Fig. 8(a). From this result, it is expected that when the passive films of the D2W and D5W alloys are locally damaged and bare matrices are exposed to the acidified chloride environments inside the pit, the active dissolution of the D5W alloy matrix will be accelerated than that of the D2W alloy, and hence repassivation of the D5W alloy will be retarded. In order words, the initiated pit or crack in the D5W alloy become easier to growth than the D2W alloy.

With increasing the W content in the Ni-saving DSSs (Fe18Cr6Mn3Mo0.4N(2.13, 5.27)W, in wt%), the repassivation of metastable pit will be restrained, and the propagation of pitting corrosion will be encouraged. Consequently, the beneficial effect of W was negligible on improving the SCC resistance in these alloys, even with the addition of impractically large amount of 5 wt% W. The present study strongly suggests that both initiation and propagation of pitting corrosion need to be considered for designing DSSs with low SCC susceptibility.

4. CONCLUSIONS

The SCC behavior of newly developed Ni-saving DSSs (Fe18Cr6Mn3Mo0.4N(2.13, 5.27)W, in wt%) was investigated in 4 M NaCl solution at 80 °C under an anodic applied potential using a SSRT method. The effect of W on the SCC susceptibility of the developed DSSs was assessed based on the SSRT results and micrographic as well as fractographic observations, and the results were discussed in terms of the electrochemical behavior of the alloys. As a result, the following conclusions could be drawn.

(1) The change in the W content from 2.13 to 5.27 wt% marginally affected the tensile properties of the investigated DSSs, which was measured in air at a strain rate of 10^{-3} s^{-1}. In both alloys, the dimpled rupture mode prevailed.

(2) Potentiodynamic polarization tests revealed that the increase in the W content from 2.13 to 5.27 wt% were effective to elevate the E_{pit} and E_{rp} of the alloys.

(3) Both alloys were susceptible to SCC in 4 M NaCl at 80 °C under an anodic applied potential. It was found that SCC resistance of the alloy was marginally improved by addition of W, which was difficult to be understood considering the significantly increased E_{pit} and E_{rp} values by addition W. The SCC resistance of the alloys should be explained by combined effects of the pit initiation probability and pit propagation rate. The slight enhancement in the SCC resistance of the

alloy by addition of W, despite the significantly decreased pit initiation probability, was correlated with the accelerated galvanic corrosion between the α and γ phases as a result of the W partitioning into the α phase, which could encourage the propagation of pitting.

ACKNOWLEDGMENTS

This work has been supported by the Engineering Research Center (ERC) Program through the National Research Foundation of Korea (NRF) funded by the Ministry of Education, Science and Technology (2013-0009451). This study was also supported financially by Fundamental Research Program of the Korean Institute of Materials Science (KIMS).

REFERENCES

1. R. M. Davison and D. Redmond, *Mater. Design* **12**, 187 (1991).
2. T. Maki, T. Furuhara, and K. Tsuzaki, *ISIJ Int.* **41**, 571 (2001).
3. J. Charles, *Steel Res. Int.* **79**, 455 (2008).
4. J. Olsson, *Desalination* **183**, 217 (2005).
5. J. Olsson and M Snis, *Desalination* **205**, 104 (2007).
6. I. Alvarez-Armas, *Recent Patents on Mechanical Engineering* **1**, 51 (2008).
7. N. R. Baddoo, *J. Constr. Steel Res.* **64**, 1199 (2008).
8. K. H. Lo, C.H. Shek, and J. K. L. Lai, *Mat. Sci. Eng. R* **65**, 39 (2009).
9. M. Snis and J. Olsson, *Desalination* **223**, 476 (2008).
10. J. Y. Choi, S. W. Hwang, M. C. Ha, and K.-T. Park, *Met. Mater. Int*. **5**, 893 (2014).
11. R. Merello, F. J. Botana, J. Botella, M. V. Matres, and M. Marcos, *Corros. Sci.* **45**, 909 (2003).
12. H. Vannevik, J. O. Nilsson, J. Frodigh, and P. Kangas, *ISIJ Inter.* **36**, 807 (1996).
13. J. O. Nilsson, G. Chai, and U. Kivisäkk, *Proc. 6th Stainless Steel Science and Market Conf.* (ed. P. Karjalainen) p. 585, European Stainless Steel Conference, Helsinki, Finland (2008).
14. L. Weber and P. J. Uggowitzer, *Mat. Sci. Eng. A* **242**, 222 (1998).
15. M. E. Wilms, V. J. Gadgil, J. M. Krougman, and F. P. Ijsseling, *Corros. Sci.* **36**, 781 (1994).
16. H. Sieurin, R. Sandstrom, and E. M. Westin, *Metall. Mater. Trans. A* **37**, 2975 (2006).
17. I. U. H. Toor, J. H. Park, and H. S. Kwon, *Corros. Sci.* **50**, 404 (2008).
18. J. Li, Z. Zhang, H. Chen, X. Xiao, J. Zhao, and L. Jiang, *Metall. Mater. Trans. A* **43**, 428 (2012).
19. L. Zhang, W. Zhang, Y. Jiang, B. Deng, D. Sun, and J. Li, *Electrochim. Acta* **54**, 5387 (2009).
20. J. Y. Choi, J. H. Ji, S. W. Hwang, and K. T. Park, *Mat. Sci. Eng. A* **528**, 6012 (2011).
21. H. Y. Ha, T. H. Lee, and B. C. Hwang, *Korean Patent* 10-1306263 (2013).
22. S. H. Kim, B. J. Song, and W. S. Ryu, *Met. Mater. Int.* **7**, 297 (2001).
23. J. Zhao, Y.W. Kim, J. H. Lee, J. M. Lee, H. S. Chang, and C. S. Lee, *Met. Mater. Int*. **18**, 217 (2012).
24. F. Abe and S. Nakazawa, *Metall. Mater. Trans. A* **23**, 3025 (1992).
25. K. M. Kim and K.Y. Kim, *J. Power Sources* **173**, 917 (2007).
26. Z. X. Zhang, Q. X. Ran, Y. L. Xu, X. J. Yu, D. W. Jiang, and X. S. Xiao, *J. Iron Steel Res. Int.* **21**, 69 (2014).
27. A. Irhzo, Y. Segui, N. Bui, and F. Dabosi, *Corros. Sci.* **26**, 769 (1986).
28. J. Chen and J. K. Wu, *Corros. Sci.* **30**, 53 (1990).
29. W.-S. Ji, Y.-W. Jang, and J.-G. Kim, *Met. Mater. Int.* **17**, 463 (2011).
30. C. J. Park and H. S. Kwon, *Corros. Sci.* **44**, 2817 (2002).
31. J. S. Kim and H. S. Kwon, *Corrosion* **55**, 512 (1999).
32. C. J. Park, M. K. Ahn, and H. S. Kwon, *Mat. Sci. Eng. A* **418**, 211 (2006).
33. K. Y. Kim, P. Q. Zhang, T. H. Ha, and Y. H. Lee, *Corrosion* **54**, 910 (1998).
34. J. S. Kim, T. H. Ha, and K.Y. Kim, *Corrosion* **57**, 452 (2001).
35. ASTM Standard G129, *Standard Practice for Slow Strain Rate Testing to Evaluate the Susceptibility of Metallic Materials to Environmentally Assisted Cracking*, vol. 03.02, Annual book of ASTM standards, PA, USA (2000).
36. R. Nishimura and Y. Maeda, *Corros. Sci.* **46**, 769 (2004).
37. Y. S. Yoon, H. Y. Ha, T. H. Lee, and S. S. Kim, *Corros. Sci.* **80**, 28 (2014).
38. Y. S. Yoon, H. Y. Ha, T. H. Lee, and S. S. Kim, *Corros. Sci.* **88**, 337 (2014).
39. E. Novak and J. Schmit, *Proc. XVII IMEKO World Congress Metrology in the 3rd Millennium*, p. 183, HMD, Croatian Metrology Soc. Dubrovnik, Croatia (2003).
40. H. Y. Ha, M.H. Jang, T. H. Lee, and J. Moon, *Corros. Sci.* **89**, 154 (2014).
41. G. S. Frankel, *J. Electrochem. Soc.* **145**, 2186 (1998).
42. T. A. Mozhi, W. A. T. Clark, and B. E. Wilde, *Corros. Sci.* **27**, 257 (1987).
43. W. T. Tsai, V. Reynders, M. Stratmann, and H. J. Grabke, *Corros. Sci.* **34**, 1647 (1993).
44. J. Congleton and W. Yang, *Corros. Sci.* **37**, 429 (1995).
45. J. I. Son, S. S. Kim, J. H. Lee, and B. H. Choi, *Metall. Mater. Trans. A* **34**, 1617 (2003).
46. Y. H. Jang, S. S. Kim, and J. H. Lee, *Mat. Sci. Eng. A* **396**, 302 (2005).
47. Z. Zhang, Z. Wang, Y. Jiang, H. Tan, D. Han, and Y. Guo, *Corros. Sci.* **62**, 42 (2012).
48. H. Hwang and Y. Park, *Mater. Trans.* **50**, 1548 (2009).
49. H. Tan, Y. Jiang, B. Deng, T. Sun, J. Xu, and J. Li, *Mater. Charact.* **61**, 1049 (2009).

50. Y. Yang, H. Tan, Z. Zhang, Z. Wang, Y. Jiang, and J. Li, *Corrosion* **69**, 167 (2013).
51. Z. Wei, J. Laizhu, H. Jincheng, and S. Hongmei, *Mat. Sci. Eng. A* **497**, 501 (2008).
52. M. Rosso, I. Peter, and D. Suani, *J. Achiev. Mater. Manuf. Eng.* **59**, 26 (2013).
53. H. Y. Ha, M. H. Jang, T. H. Lee, and J. Moon, *Mater. Charact.* **106**, 338 (2015).
54. L. F. Garfias-Mesias, J. M. Syke, and C. D. S. Tuck, *Corros. Sci.* **387**, 1319 (1996).
55. S. T. Kim, I. S. Lee, J. S. Kim, S. H. Jang, Y. S. Park, K. T. Kim, and Y. S. Kim, *Corros. Sci*. **64**, 164 (2012).
56. R. Newman, *Electrochem. Soc. Interface* **19**, 33 (2010).
57. H. Y. Ha, T. H. Lee, and S. J. Kim, *Electrochim. Acta* **80**, 432 (2012).
58. L. Q. Guo, M. Li, X. L. Shi XL, X. Yan, X. Y. Li, and L. J. Qiao, *Corros. Sci.* **53**, 3733 (2011).